Molecular BioSystems

Cite this: *Mol. BioSyst.*, 2012, **8**, 1824–1832

www.rsc.org/molecularbiosystems

PAPER

Rewiring and dosing of systems modules as a design approach for synthetic mammalian signaling networks†

Michael M. Kämpf,‡[a] Raphael Engesser,‡[bc] Moritz Busacker,[d] Maximilian Hörner,[cde] Maria Karlsson,[ad] Matias D. Zurbriggen,[cd] Martin Fussenegger,[a] Jens Timmer[bcefg] and Wilfried Weber*[acdef]

Received 23rd December 2011, Accepted 31st March 2012
DOI: 10.1039/c2mb05509k

Modularly structured signaling networks coordinate the fate and function of complex biological systems. Each component in the network performs a discrete computational operation, but when connected to each other intricate functionality emerges. Here we study such an architecture by connecting auxin signaling modules and inducible protein biotinylation systems with transcriptional control systems to construct synthetic mammalian high-detect, low-detect and band-detect networks that translate overlapping gradients of inducer molecules into distinct gene expression patterns. Guided by a mathematical model we apply fundamental computational operations like conjunction or addition to rewire individual building blocks to qualitatively and quantitatively program the way the overall network interprets graded input signals. The design principles described in this study might serve as a conceptual blueprint for the development of next-generation mammalian synthetic gene networks in fundamental and translational research.

Introduction

The fate and function of complex biological systems is controlled by modularly organized signaling networks interpreting physiological and environmental cues to orchestrate the organism's gene expression profile.[1–3] In such organization vertices divide into groups that are further sub-structured into groups of groups over multiple levels. Individual groups in these networks take over modular functions like the perception or amplification of a signal, the metabolic conversion of a substrate into a product[4] or the transcriptional modulation of a gene regulatory network.[3] The clustering of the individual groups yields an overall complex phenotype the characteristics of which can be tuned by changing the network's connectivity.[3] Recent work suggests that such rewiring of individual network components represents a major source for evolutionary novelty.[5,6] In these processes most network modules are functionally conserved, however, a few modules gain novel connectivity by the specific interaction with another protein[7] or an alternatively connected gene expression control.[8] For example, it has been shown that changes in network connectivity as introduced by transposons[8,9] are involved in sex determination,[8] in the evolution of pregnancy in mammals[9] or of animal body plans.[10]

The functional basis of such networks are individual regulatory modules that control receptor-based signaling, phosphorylation- and second messenger-mediated cascades or genetic and epigenetic transcription control systems.[6,10,11] A recently discovered example for such a regulatory module is the receptor TIR1 for the plant hormone auxin. Binding of auxin to TIR1 triggers heterodimerization with Aux/IAA transcriptional repressors that are subsequently targeted for degradation through the action of the SCF^{TIR1} E3 ubiquitin ligase.[12] As the SCF degradation pathway is conserved among eukaryotes, the ectopic expression of TIR1 was shown to be sufficient to degrade Aux/IAA-containing proteins in an auxin-inducible manner in mammalian, avian and yeast cells.[13]

Another common motif in regulatory networks is the covalent modification of signaling proteins for instance *via* phosphorylation, which impacts protein function and interaction with other partners. A recently described synthetic emulation of regulatory protein modification relies on the inducible biotinylation of target proteins and their subsequent dimerization with streptavidin-containing binding partners. For example it was shown that the biotin-inducible reconstitution of split synthetic transcription factors could be used to

[a] *Department of Biosystems Science and Engineering, ETH Zurich, Mattenstrasse 26, 4058 Basel, Switzerland*
[b] *Faculty of Physics, University of Freiburg, Hermann-Herder-Str. 3, 79104 Freiburg, Germany*
[c] *BIOSS Centre for Biological Signalling Studies, University of Freiburg, Hebelstrasse 25, 79104 Freiburg, Germany*
[d] *Faculty of Biology, University of Freiburg, Schänzlestrasse 1, 79104 Freiburg, Germany. E-mail: wilfried.weber@biologie.uni-freiburg.de; Fax: +49 761 203 97660; Tel: +49 761 203 97654*
[e] *Spemann Graduate School of Biology and Medicine SGBM, University of Freiburg, Albertstrasse 19a, 79104 Freiburg, Germany*
[f] *ZBSA Center for Biological Systems Analysis, University of Freiburg, Habsburgerstr. 49, 79104 Freiburg, Germany*
[g] *FRIAS Freiburg Institute for Advanced Studies, University of Freiburg, Albertstrasse 19, 79104 Freiburg, Germany*
† Electronic supplementary information (ESI) available. See DOI: 10.1039/c2mb05509k
‡ Both authors contributed equally to this study.

construct a synthetic network allowing time-delayed transgene expression in mammalian cells.[14]

The most versatile motif to exert control on cellular function relies on synthetic gene switches based on small molecule-responsive DNA-binding proteins. Fusing such proteins to transcriptional activation or silencing domains could be used to regulate the activity of minimal or constitutive promoters in a ligand-dependent manner.[15] Following this design principle, synthetic gene switches were developed that enabled the induction or silencing of transgene activity in response to different drugs like tetracycline, macrolide or streptogramin antibiotics[16–18] or to metabolites such as amino acids, antioxidants and vitamins.[19]

In this study we follow a model-based approach to understand how such individual regulatory modules can be connected to networks performing desired complex computational operations and how the connectivity and dosage of the individual parts determine the overall network characteristics. With the example of networks that translate concentration gradients of a signaling molecule into distinct gene expression patterns, we show that the network performance can quantitatively and qualitatively be tuned by changing its dosage and connectivity rather than the molecular properties of the underlying modular building blocks. As it is significantly easier to change dosage and connectivity rather than engineering the molecular properties of the underlying proteins (*e.g.* by mutagenesis), this study provides important design approaches for the realization of next-generation synthetic mammalian networks.

Results

Model-based design and construction of networks interpreting the concentration of inducer molecules

We first analyzed how the connection of two control modules, plant hormone signaling and gene expression control can lead to the emergence of complex behavior as exemplified by the design of a band-detect network responsive only to a narrow concentration range of the plant morphogen auxin. Such band-detect systems playing essential roles in morphogenesis and development[20,21] can be constructed by superimposing a low-detect and a high-detect filter in a manner that the cut-off areas of both devices are not overlapping.[20–22] We first devised a low-detect filter by combining the tetracycline-responsive transactivator tTA[17] with an Aux/IAA17-derived degron domain (AID[13]) conferring tTA–AID ubiquitylation and proteasomal degradation at elevated auxin concentrations (Fig. 1A). For this aim tTA–AID was placed under the control of its cognate promoter P_{TET} to result in a positive feedback loop configuration[23] the activity of which was quantified by a P_{TET}-driven SEAP (human placental secreted alkaline phosphatase) reporter construct. Transfecting this system together with a TIR1 expression plasmid into human embryonic kidney cells (HEK-293T) and exposing the cells to increasing auxin concentrations resulted in high SEAP expression levels at auxin concentrations <19 μM and gradually decreasing the SEAP output when increasing the auxin input (Fig. 1A).

For the construction of the high-detect filter we inverted the functionality of the above-described low-detect device by replacing the transactivator tTA with the transcriptional silencer E-KRAB.[18] The resulting E-KRAB–AID silenced

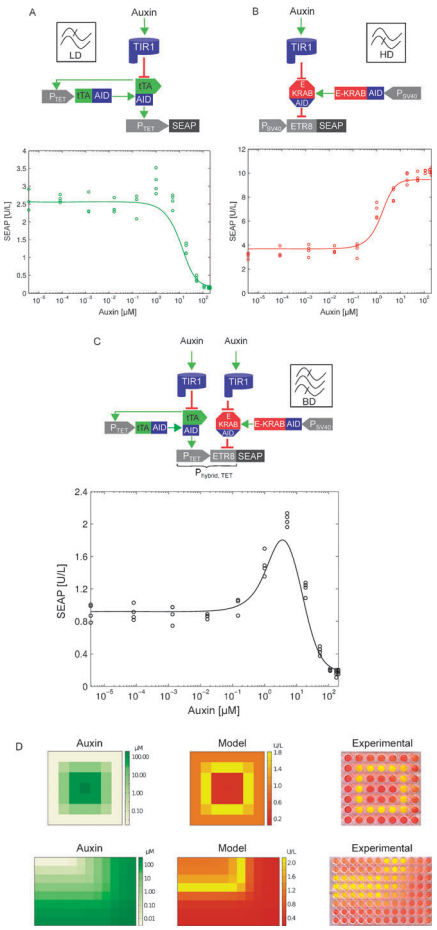

Fig. 1 Modular design and construction of a synthetic band-detect network by the superposition of a low- and a high-detect filter. (A) Design and construction of the low-detect filter. The tetracycline transactivator tTA is fused to the auxin-inducible degradation domain (AID) and expressed in a positive feedback loop configuration under the control of the tTA-responsive promoter P_{TET}. P_{TET} is further configured to drive expression of the reporter gene SEAP (secreted alkaline phosphatase). This filter was implemented in HEK-293T cells and subjected to increasing auxin concentrations for 48 h prior to SEAP quantification. The green line represents the fit of the mathematical model to the experimental data (green circles). (B) Design and construction of the high-detect filter. The macrolide-responsive repressor E-KRAB is fused to the auxin-inducible degradation domain AID and expressed under the control of the simian virus 40 promoter P_{SV40}. E-KRAB–AID binds to its cognate operator sequence ETR8 and represses SEAP production. This system was cotransfected into HEK-293T cells and exposed to increasing auxin concentrations for 48 h prior to the quantification of SEAP production. The red line represents the model fit to the experimental SEAP values (red circles). (C) Design and construction of the band-detect network. The low- (Fig. 1A) and high- (Fig. 1B) detect filters were superposed to a band-detect network by combining the output signals of each single module *via* a hybrid promoter ($P_{TET,Hybrid}$, activated by tTA–AID *via* P_{TET} and repressed by E-KRAB–AID *via* ETR8). The black line represents the model prediction for SEAP production based on the model parameterization of the individual low- and high-detect filters (Fig. 1A and B), the black circles represent the experimentally obtained SEAP values. (D) Band-detect type interpretation of a two-dimensional auxin gradient. The band-detect network was applied to interpret one concentric or two orthogonally overlapping gradients. The model-predicted and the experimentally observed expression patterns of the SEAP reporter are shown. SEAP production is visualized by the incubation with *para*-nitrophenyl phosphate resulting in a yellow color output.

the reporter gene SEAP placed under the control of a simian virus 40 promoter (P_{SV40}) fused to an octameric E-KRAB–AID-responsive operator site (ETR8) (Fig. 1B). Co-transfecting this reporter construct together with an E-KRAB–AID and TIR1 expression vector into HEK-293T cells resulted in high SEAP production only at auxin concentrations >1 μM (Fig. 1B).

In order to gain a quantitative understanding of these low- and high-detect systems and to enable the rational and predictive engineering and combination of both systems we developed a mathematical model based on ordinary differential equations. The low detect device (Fig. 1A) can be described by eqn (1)–(3).

$$\frac{d[\text{tTA}-\text{AID}]}{dt} = b_1 - (k_1 + k_3[C]_{eq})[\text{tTA}-\text{AID}] + k_2\frac{[\text{tTA}-\text{AID}]^2}{K_{m1}^2 + [\text{tTA}-\text{AID}]^2} \quad (1)$$

$$\frac{d[\text{SEAP}]}{dt} = b_3 + k_6\frac{[\text{tTA}-\text{AID}]^2}{K_{m2}^2 + [\text{tTA}-\text{AID}]^2} \quad (2)$$

with

$$[C]_{eq} = \frac{f[\text{AUX}]_0 + [\text{TIR1}]_0 + K}{2} - \sqrt{\left(\frac{f[\text{AUX}]_0 + [\text{TIR1}]_0 + K}{2}\right)^2 - f[\text{AUX}]_0[\text{TIR1}]_0} \quad (3)$$

In this model the production rate of tTA–AID under the control of P_{TET} is described *via* Monod kinetics (Monod constant K_{m1}) where k_2 is the promoter strength under fully induced conditions and b_1 is the basal activity in the uninduced state. tTA degradation is described by a linear degradation term k_1 and by the auxin-induced TIR1-dependent degradation represented by the rate $k_3[C]_{eq}$. $[C]_{eq}$ describes the steady state concentration of the TIR1–auxin complex depending on the initial concentrations of the TIR1 receptor $[\text{TIR1}]_0$ and of auxin $[\text{AUX}]_0$. The corresponding eqn (3) can be deduced from mass action kinetics where K is the dissociation constant of the TIR1–auxin binding process and f is the fraction of auxin which is imported into the cell as described in more detail in ESI†. The SEAP production rate under control of the P_{TET} promoter is described by the basal production rate b_3 and by Monod kinetics (Monod constant K_{m2}) with k_6 being the production rate under fully induced conditions. SEAP degradation was neglected in the model as the half-life of SEAP is 502 h[24] which is significantly above the time-scales of the present study. As tTA binds as a dimer cooperatively to P_{TET}[25] we introduced the Hill coefficient $n = 2$ for tTA–AID binding of P_{TET}.

The high-detect filter can be described by eqn (4) and (5).

$$\frac{d[\text{E-KRAB}-\text{AID}]}{dt} = b_2 - (k_4 + k_5[C]_{eq})[\text{E-KRAB}-\text{AID}] \quad (4)$$

$$\frac{d[\text{SEAP}]}{dt} = \frac{b_4}{1 + k_7[\text{E-KRAB}-\text{AID}]^2} \quad (5)$$

The repressor E-KRAB–AID is constitutively expressed by the promoter P_{SV40} with the rate b_2 (eqn (4)). The degradation terms are similar to eqn (1). The expression of the target gene SEAP is regulated by an allosteric inhibition whose strength is determined by k_7. As E-KRAB–AID binds its operator ETR8 cooperatively as dimer[26] we introduced the Hill coefficient $n = 2$ into eqn (5).

In the next step we applied this model to evaluate whether a superposition of the low- and high-detect filters would result in the desired band-detect characteristics. Therefore we modeled a superposition of both devices by designing a hybrid promoter for SEAP expression responsive to both synthetic transcription factors, tTA–AID and E-KRAB–AID with the repressor being dominant over the activator (Fig. 1C). The resulting SEAP production rate can be described by combining eqn (2) and (5) to eqn (6).

$$\frac{d[\text{SEAP}]}{dt} = b_3 + \frac{k_6}{1 + k_7[\text{E-KRAB}-\text{AID}]^2}\frac{[\text{tTA}-\text{AID}]^2}{K_{m2}^2 + [\text{tTA}-\text{AID}]^2} \quad (6)$$

In order to predict systems performance, we parameterized the model based on the experimental data shown in Fig. 1A and B (see ESI†) and on literature data.[25] The model predicted that the superposition of the low- and the high-detect systems should result in band-detect characteristics (Fig. 1C) with maximum SEAP expression at auxin concentrations of 5 μM.

In order to experimentally validate the model predictions we cloned the SEAP gene under the control of a hybrid promoter ($P_{hybrid,TET}$) composed of the tTA–AID-responsive P_{TET} promoter with an additional insertion of an octameric E-KRAB–AID-specific operator site[25] (ETR8, Fig. 1C). Co-transfection of this reporter construct with expression vectors for tTA–AID, E-KRAB–AID and TIR1 into HEK-293T cells exposed to increasing auxin concentrations resulted in an expression peak the shape and position of which match with high precision to the model predictions (Fig. 1C).

The model analysis further predicted that this synthetic band-detect network could be used to interpret two-dimensional gradients to result in spatially restricted gene expression patterns. For example, the band detect-type interpretation of a concentric gradient resulted in ring-shaped gene expression patterns while two orthogonally superimposed gradients resulted in the delineation of one quadrant of the experimental space (Fig. 1D and Table S6 (ESI†) for quantitative data).

Analyzing and tuning the network output

Next we performed a model-based analysis to investigate the function of individual modules with the aim to identify actuating variables suitable to tune the characteristics of the band-detect network.

According to eqn (6) the response characteristics of the band-detect network depend on the relative effect of the silencing (E-KRAB–AID) and the activating (tTA–AID) transcription factors on the target hybrid promoter. These effects can be attributed to (i) the TIR1-mediated auxin-dependent transcription factor degradation (represented by $[C]_{eq}$, eqn (3)), (ii) the auxin/TIR1-independent transcription factor production and degradation as well as (iii) the effect of the transcription factors on the target hybrid promoter. In the following we analyzed the effect of the transcription factors according to those three criteria.

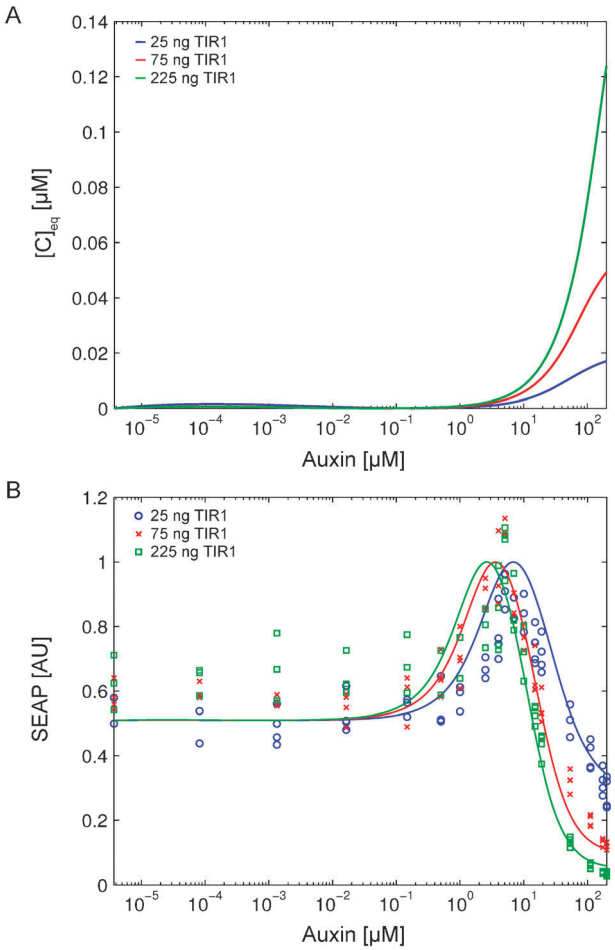

Fig. 2 Tuning network performance. The effect of the TIR1 concentration. (A) Influence of TIR1 concentration on $[C]_{eq}$. The equilibrium concentration of the auxin–TIR1 $[C]_{eq}$ complex was modeled as a function of the initial auxin concentration in the gradient. (B) Influence of TIR1 concentration on band-shift network characteristics. The band-detect network (Fig. 1C) was subjected to an auxin gradient using increased or decreased TIR1 expression plasmid amounts for co-transfection. The lines indicate the model-predicted SEAP expression profiles and the symbols represent the experimentally obtained SEAP values.

In order to analyze the impact of the auxin/TIR1-dependent degradation, we investigated the dependence of $[C]_{eq}$ as a function of auxin and TIR1 concentrations (Fig. 2A). At low auxin concentrations (<1 μM) all auxin is bound to its receptor TIR1 and therefore $[C]_{eq}$ is independent of [TIR1]. However, at high auxin concentrations (>19 μM) TIR1 becomes limiting thereby resulting in a direct proportionality of $[C]_{eq}$ with [TIR1]. Based on these findings we modeled the performance of the band detect network as a function of the TIR1 concentration (Fig. 2B). At increasing auxin concentrations (>20 μM) high TIR1 levels lead to an abrupt drop in SEAP production whereas lower TIR1 levels yielded a broader peak shape and a shift in the peak position to higher auxin values. However, at low auxin concentrations (<1 μM) the amount of the TIR1–auxin complex $[C]_{eq}$ is not affected, thus no change in the network output was predicted. This [TIR1]-dependent behavior was verified in the experimental system by increasing or decreasing the original amount (75 ng) of the TIR1 expression plasmid in the transfection mix by a factor of 3 revealing a good match between experimental data and model prediction (Fig. 2B).

In the next step we analyzed the auxin/TIR1-independent contribution of the transcription factor concentrations to the band-detect characteristics.

In order to analyze the impact of E-KRAB–AID, we investigated the analytical solution of eqn (4) which describes the time evolution of E-KRAB–AID with the starting concentration of [E-KRAB–AID](0) = 0:

$$[\text{E-KRAB} - \text{AID}](t) = \frac{b_2}{k_4 + k_5[C]_{eq}}(1 - e^{-(k_4+k_5[C]_{eq})t}). \quad (7)$$

In eqn (7) the E-KRAB–AID concentration scales linearly with b_2. As a linear scaling of the concentration of E-KRAB–AID leads to a shift in the cut-off area of the high-detect filter (eqn (5)), changing b_2 is expected to result in a shifted position of the band-detect peak. The parameter b_2 can be tuned by varying the amount of the E-KRAB–AID expression plasmid in the transfection mix (Fig. 3A).

For investigating the impact of tTA–AID, we analyzed numerical simulations of eqn (1) that is analytically non-solvable. These simulations revealed that changing the amount of the tTA–AID expression plasmid was expected to lead to a shift of the edge from the low-detect filter (Fig. 3B).

Combining both effects, a model-based analysis predicted that higher plasmid amounts for both transcription factors should lead to a shift of the peak maximum to higher auxin concentrations whereas lower amounts of both plasmids should shift the peak to lower auxin concentrations. This model-predicted behavior was experimentally verified by lowering the expression vector amount for tTA–AID and E-KRAB–AID from 97.5 to 45 ng per cell culture well (Fig. 3C). In accordance with the model prediction the experimentally observed SEAP peak shifted from 5 μM auxin to 2.5 μM for the lower tTA–AID and E-KRAB–AID plasmid amounts (Fig. 3A–C). Similarly, by only varying the concentration of one transcription factor, peak symmetry can be adjusted. Increasing the concentration of E-KRAB–AID by 1.5-fold resulted in more symmetrical SEAP expression values in both low states (Fig. 3D).

The effect of the transcription factors on the hybrid promoter was analyzed by replacing the tetracycline-responsive repressor TetR in tTA–AID (TetR–VP16–AID; VP16, *Herpes simplex*-derived transactivation domain) with the *Streptomyces coelicolor*-derived quorum-sensing repressor ScbR[27] thus resulting in the chimeric transcription factor SCA–AID (ScbR–VP16–AID). Accordingly, the tetracycline promoter P_{TET} in $P_{hybrid,TET}$ was exchanged for the SCA-responsive promoter P_{ScbR} thereby resulting in the hybrid promoter $P_{hybrid,ScbR}$ (Fig. 4A; Fig. S1, ESI†). As P_{ScbR} harbors only one binding site for SCA dimers[27] instead of the seven tTA dimer binding sites in P_{TET},[17] P_{ScbR} is a weaker promoter than P_{TET}. Integrating the weaker SCA–AID system into the model resulted in a SEAP peak shifted from 5 μM auxin to 1 μM auxin as subsequently confirmed by experimental data (Fig. 4B). This peak shift which was achieved by using the two mutually compatible transcription factors tTA–AID and SCA–AID also enabled the formation of two distinct expression patterns controlled by one auxin gradient. Such a process was

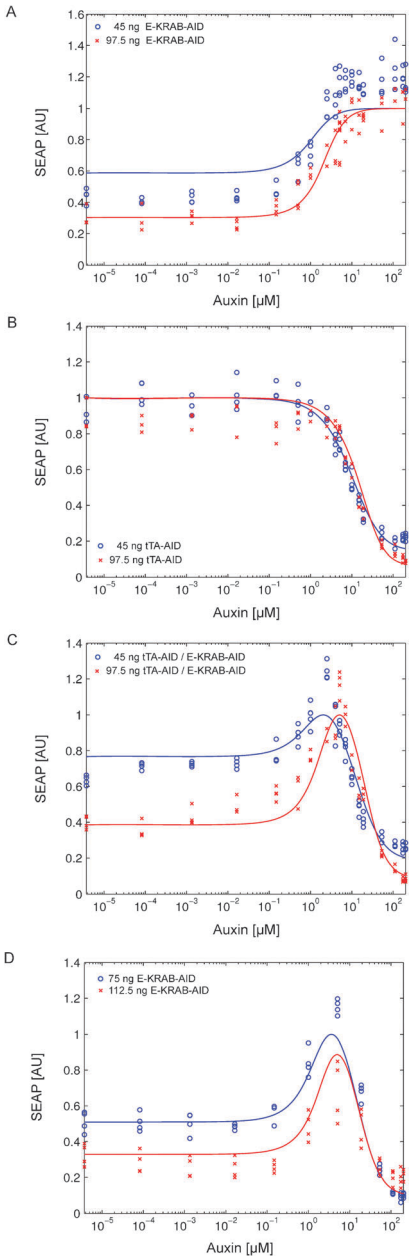

Fig. 3 Tuning network performance. The effect of the transcriptional activator and repressor concentrations. (A) Analysis of the high-detect filter. The high-detect filter (Fig. 1B) was subjected to an auxin gradient using low (45 ng) or high (97.5 ng) amounts of the E-KRAB–AID expression plasmid in the transfection mix. The lines represent the model fit to the experimentally observed SEAP output values (symbols). (B) Analysis of the low-detect filter. The low-detect filter (Fig. 1A) was subjected to an auxin gradient using low (45 ng) or high (97.5 ng) amounts of the tTA–AID expression plasmid in the transfection mix. The lines represent the model fit to the experimentally observed SEAP output values (symbols). (C) Analysis of the band-detect network. The high- and low-detect filters (Fig. 3A and B) using different transcriptional activator and repressor concentrations were combined to a band-detect network (network shown in Fig. 1C) and subjected to an auxin gradient. The model-predicted (lines) and experimentally obtained (symbols) SEAP production values are shown. (D) Tuning peak symmetry. The E-KRAB–AID plasmid amount in the band-detect network was increased 1.5-fold (compared to Fig. 1C). The model-predicted (lines) and experimentally obtained (symbols) SEAP production values are shown.

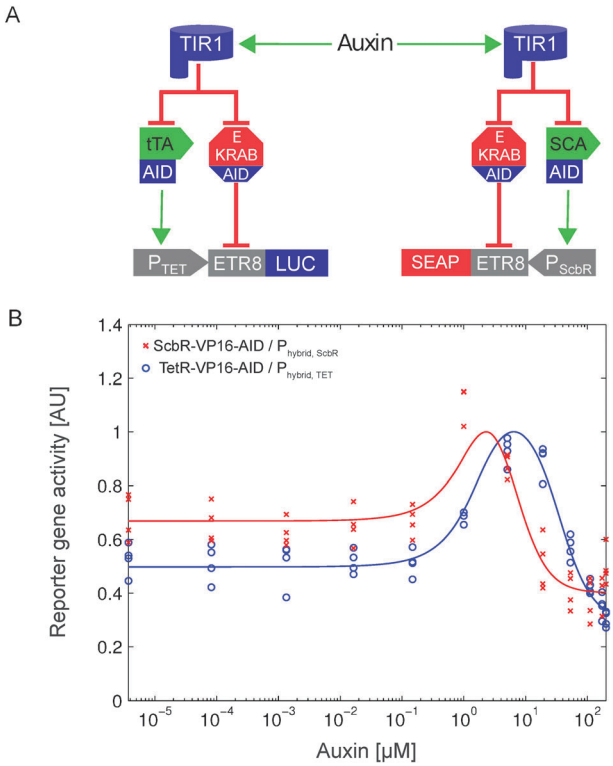

Fig. 4 Tuning network performance. The effect of the transactivator–promoter interaction. (A) Design of the band-detect network using different activator–promoter pairs. The band-detect network was implemented using either the tTA–AID or the *Streptomyces coelicolor*-derived SCA–AID transactivators in combination with the respective target promoters $P_{hybrid,TET}$ or $P_{hybrid,ScbR}$. For discrimination between both systems $P_{hybrid,TET}$ was configured to drive expression of firefly luciferase. (B) Modeling and implementation of the band-detect network using different transactivator–promoter pairs. The band-detect networks relying on tTA–AID or SCA–AID (Fig. 4A) were subjected to an auxin gradient and the experimental data (symbols) as well as the model fit (lines) are shown.

realized by combining the tTA–AID and SCA–AID-based systems. For discrimination between both networks, the promoter $P_{hybrid,TET}$ was coupled to firefly luciferase instead of SEAP. Co-transfecting both systems into HEK-293T cells subjected to increasing auxin concentrations resulted in two distinct expression peaks of SEAP and luciferase at auxin concentrations of 1 and 5 μM, respectively (Fig. 4B).

Introduction of a biotin-based band-detect network

The formation of complex spatial patterns in nature commonly relies on networks simultaneously interpreting multiple morphogen gradients.[28] In order to analyze how the topology of regulatory networks determines how such gradients are translated into distinct gene expression patterns, we introduced biotin as a second inducer. Increasing biotin concentrations can be interpreted with band-detect characteristics by the use of a biotin-dependent split transcription factor composed of the *Herpes simplex* VP16 transactivation domain fused to the biotinylation signal avitag and the streptogramin-responsive repressor PIP fused to biotin-binding streptavidin[14,29] (SA, Fig. 5A). In the absence of biotin, dimerization of both

protein domains is prevented, however at increasing biotin concentrations (>0.5 nM biotin) avitag is biotinylated by co-expressed biotin ligase BirA thus enabling the heterodimerization with PIP–SA. When further increasing the biotin concentration above 2.7 μM, SA is gradually saturated by free biotin thereby competitively preventing the dimerization with biotinylated avitag–VP16. Only upon dimerization of PIP–SA with biotinylated avitag–VP16 a functional transcription factor is reconstituted that can activate SEAP transcription from the PIP-responsive promoter P_{PIR8}.[29,30] The functionality of the system was analyzed in HEK-293T cells (for expression vectors see Fig. S1, ESI†) subjected to a biotin gradient. Only at intermediate biotin concentrations high SEAP production was observed with a peak at 0.03 μM biotin thereby confirming band-detect characteristics. By adapting and fitting a previous model on biotin-dependent time-delayed gene expression[14] to the specific molecular components used in this study, we obtained a quantitative description of the biotin-dependent band-detect network (Fig. 5B and ESI† for details on the model).

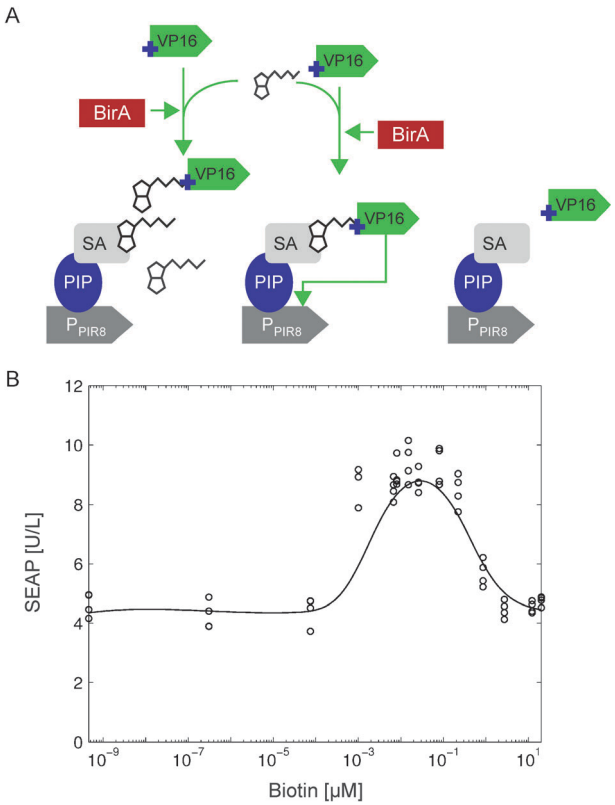

Fig. 5 Design and characterization of a biotin-dependent band-detect network. (A) Design of the biotin-dependent band-detect network. A biotin-dependent transcription factor was designed by fusing streptavidin (SA) to the *Streptomyces pristinaespiralis*-derived repressor PIP that binds its cognate promoter P_{PIR8}. In the presence of biotin co-expressed biotin ligase BirA biotinylates the avitag-sequence (blue cross) fused to the *Herpes simplex*-derived transactivator VP16. At low biotin concentrations (right) VP16 is not biotinylated thereby preventing the reconstitution of the chimeric growth factor. However, at intermediate biotin levels (middle) VP16 is biotinylated and bound to PIP–SA thereby activating the target promoter P_{PIR8} whereas further biotin addition outcompetes Biotin–VP16 binding to SA (left). (B) Functional analysis of the biotin-dependent band-detect network. The biotin-dependent band-detect network was subjected to a biotin gradient. The experimentally observed (circles) SEAP output and the corresponding model fit (solid line) are indicated.

Changing network functionality by rewiring the connectivity of the regulatory modules

For quantitatively understanding how changes in the connectivity of individual regulatory modules determine overall system functionality, we rewired the modules of the auxin- and biotin-dependent band-detect networks with each other following fundamental computational operations. Using a model-based approach we explored three types of network rewiring: (i) we additively rewired the output of the auxin- and biotin-responsive band-detect networks, (ii) we rewired the output of the auxin- and biotin-responsive band-detect networks following a conjunction-type operation or (iii) we directly connected the auxin-responsive low-detect filter with the biotin-responsive band-detect network in an AND-type operation and processed the output of this combined system in an additive manner with the auxin-responsive band-detect network.

For realizing the first approach, we additively combined the auxin (Fig. 1C)- and biotin (Fig. 5)-responsive band-detect networks to interpret antiparallelly or orthogonally oriented inducer molecule gradients. While the antiparallel alignment of the two gradients triggered the emergence of a striped structure reminiscent to the segmentation in the developing embryo, two orthogonally oriented gradients resulted in a cross-shaped pattern (Fig. 6A, Table S7, ESI†, for quantitative data).

In the second approach we combined the outputs of the auxin- and biotin-dependent band-detect networks in a conjunction-type configuration (Fig. 6B and Fig. S2, ESI†, for detailed network connectivity). For this aim, the output promoters of both systems $P_{hybrid,TET}$ and P_{PIR8} were fused to split fragments of firefly luciferase engineered with an FKBP/FRB-based heterodimerization system.[31] In this configuration the output signal is only active if both individual band-detect networks operate under induced conditions. When applying this combined network to two orthogonally overlapping auxin and biotin gradients, a signal is observed only in the centre where the action spectra of both networks overlap (Fig. 6B, Table S8, ESI†, for quantitative data).

In the third approach we directly rewired the auxin-responsive low-detect filter (Fig. 1A) with the biotin-dependent band-detect network (Fig. 5) in a conjunction-type operation and additively connected this system to the auxin-responsive band-detect network (Fig. 6C and Fig. S3, ESI†, for the detailed network connectivity). For this rewiring we fused the auxin-inducible degradation domain to the biotin-responsive activator avitag–VP16 thereby preventing biotin-induced gene expression at elevated auxin concentrations. This rewiring produces a conjunction-type operation. When additively combining this operation with the native auxin-responsive band-detect network, two orthogonally overlapping biotin and auxin gradients are interpreted by a T-shape-like structure (Fig. 6C, Table S9, ESI†, for quantitative data).

The networks designed in this study illustrate the potential to produce a large quantitative and qualitative diversity of signal processing capabilities by changing the dosage and connectivity of individual network building blocks. We have demonstrated that the systems output can quantitatively be

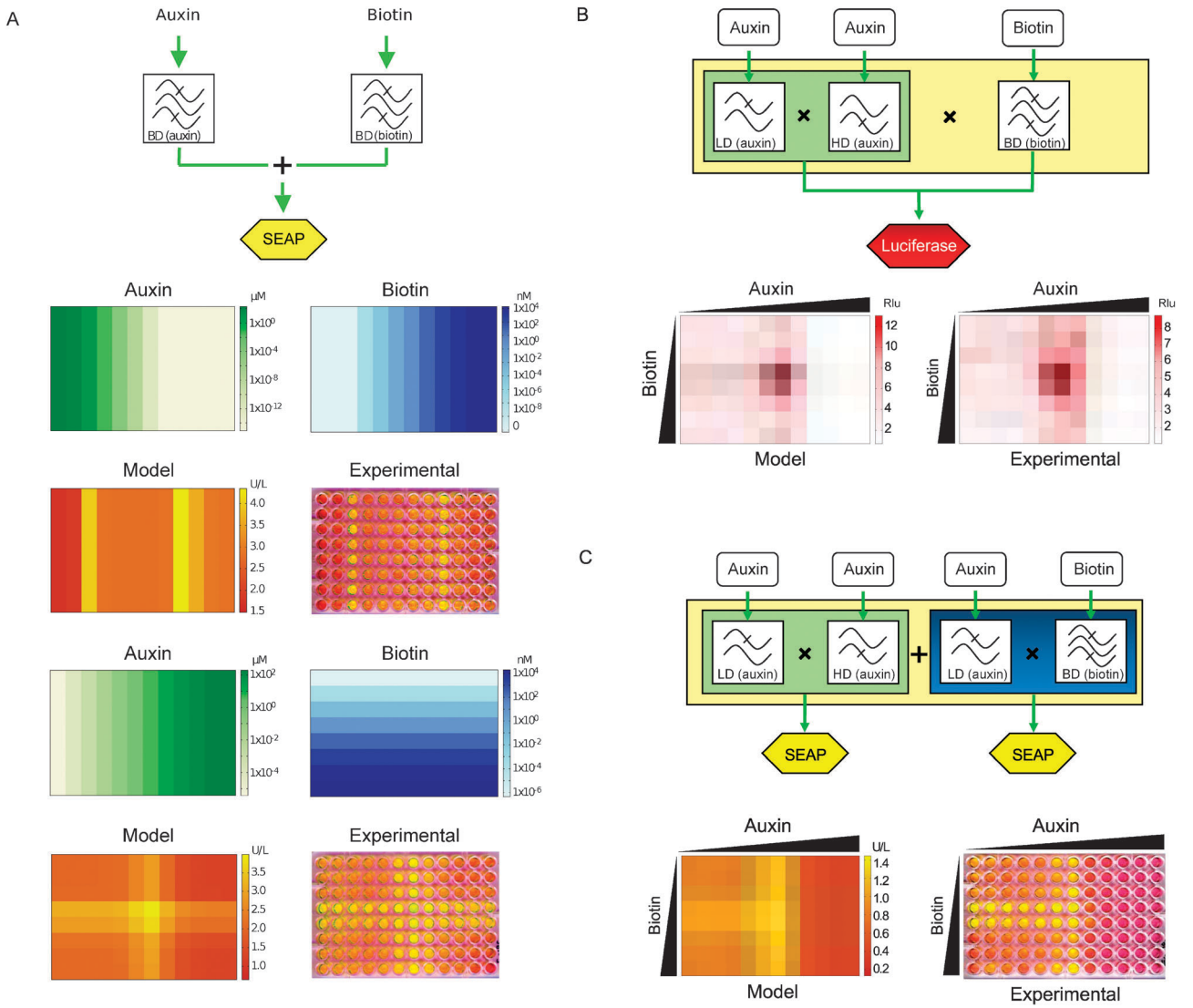

Fig. 6 Changing network functionality by rewiring the connectivity of individual network modules. (A) Additive rewiring of the auxin- and biotin-responsive band-detect networks. The auxin- and biotin-responsive band-detect networks were additively connected and applied to interpret two anti-parallel (upper panel) or orthogonal (lower panel) auxin and biotin gradients. The model-predicted and experimentally observed system responses are indicated. SEAP production is visualized by the incubation with *para*-nitrophenyl phosphate resulting in a yellow color output. (B) Conjunctive rewiring of the auxin- and biotin-responsive band-detect networks. The auxin- and biotin-responsive band-detect networks were connected in a conjunction-type configuration and applied to interpret orthogonally oriented auxin and biotin gradients (same as in Fig. 6A). The model-predicted and experimentally observed system responses as expressed by luciferase activity are shown (Rlu, relative light units). The detailed network connectivity is shown in Fig. S2 (ESI†). (C) Direct functional interconnection of auxin- and biotin-based control modules. The auxin-responsive low-detect filter was rewired with the biotin-triggered band-detect network in a conjunction-type operation. This rewired network was additively superposed to the auxin-dependent band-detect network and applied to interpret two orthogonally oriented auxin and biotin gradients (same as in Fig. 6A). The model-predicted and the experimentally observed system responses as expressed by SEAP activity are indicated. SEAP production is visualized by the incubation with *para*-nitrophenyl phosphate resulting in a yellow color output, detailed network connectivity is shown in Fig. S3 (ESI†).

predicted by mathematical modeling and that the model can thus be applied to identify network parameters for dosage and connectivity that can subsequently be adjusted to yield in overall desired network performance.

Discussion

In this study we have modularly rewired low-, high- and band-detect filters for the construction of synthetic signaling networks interpreting gradients of inducer molecules into distinct gene expression patterns. The networks in this study are based on modules at three different signaling levels, protein modification, protein degradation and inducible gene expression control. As each of these levels relies on different molecular mechanisms without direct interaction, these modules can be considered as orthogonal and can therefore be interconnected with each other to desired network topologies. This modularity and orthogonality enables us to mathematically simulate the contribution of individual modules on overall functionality in order to rapidly identify parameters by which the network

performance can quantitatively and qualitatively be engineered. The quantitative characteristics of the network were engineered by adjusting the dosing of one or several individual network modules which enabled changing the peak position, the shape of the peak as well as its symmetry. A key module in the auxin-responsive high- and band-detect filters is the synthetic repressor protein E-KRAB–AID, the dosing of which was shown to impact transgene repression at low auxin concentrations. Accordingly, increasing the amount of E-KRAB–AID increased the symmetry of the peak and reduced leaky transgene expression in the band-detect configuration.

While the dosing of individual modules enabled us to quantitatively adjust network performance, the alternative rewiring of the modules enabled us to program how the network qualitatively interpreted gradual concentrations of the input molecules. By rewiring the modules according to fundamental computational operations like addition or conjunction it was possible to interpret the same set of gradients to desired gene expression patterns.

Such synthetic networks with complex band-detect functionality might be applied to re-engineer natural developmental processes, where polarity of a developing organism is first determined by monotone gradients that are subsequently interpreted into spatially restricted, segmented gene expression patterns to determine the further lineage of the cells in each region.[28] The synthetic band-detect networks developed in this study exhibit a dynamic output range in line with one of the natural decision making processes, for example, the decision whether a mouse embryonic stem cell is committed for self-renewal or is driven into differentiation. For instance, it has been shown that variations in the expression level of *oct3/4* by ±50% of the normal diploid level were sufficient to commit pluripotent stem cells for differentiation.[32]

Beyond possible applications in re-engineering developmental processes, the network motifs described in this study rather represent a general blueprint for the construction of future synthetic biological systems: the regulatory modules in the networks described here represent the most prominent signal-transduction mechanisms like protein modification, protein degradation and transcription control. As most of the available mammalian synthetic biological tools fall within one of these categories,[33] the engineering principles described in this work are likely to be widely applicable in synthetic biology. Furthermore, the here-described approaches to quantitatively and qualitatively engineer network properties by dosing and rewiring network components are in line with natural biological processes, where major steps in evolution were realized by changes in network connectivity rather than by the *de novo* generation of building blocks.[8–10] This suggests that the principles described in this study represent a general approach for designing the next generation of mammalian synthetic networks applicable in fundamental and translational research.

Materials and methods

Expression vectors

The configurations of all vectors are shown in Fig. S1 (ESI†). The expression vector pMK210 (P_{SV40}–E-KRAB–AID–pA) was constructed by PCR-mediated amplification of E-KRAB from pWW43[18] (oligos OMK228, 5′-ccacgaattccaccatgccccg-ccccaagctcaag-3′ and OMK225, 5′-cagcacgcgtatcgatgctagccca-gagatcattccttgccattccttc-3′) and of AID from pNHK60[13] (oligos OMK226, 5′-gctagcatcgatacgcgtgctggtgcaggcgctggag-3′ and OMK229, 5′-gcctcgagaagcttttaaaccttacgtttcttttttagggacctttc-3′). Both PCR fragments were subsequently joined by PCR (oligos OMK228 and OMK229) and cloned (*Eco*RI/*Hin*dIII) into pSAM200.[16] Plasmid pMK52 ($P_{eF1\alpha}$–TIR1–pA) was constructed by amplifying TIR1 from pNHK60 (oligos OMK60, 5′-ccacgaattcccaccatgacgtacttcccggaggag-3′ and OMK61, 5′-ggtgtctagattacagatcttcttcagaaataagtttttgttctaggattttaacaaaat-ttggtgcatcatccctc-3′) and subsequent cloning (*Eco*RI/*Xba*I) into pWW29.[18] Plasmid pMK209 (P_{TET}–tTA–AID–pA) was constructed by transferring P_{TET} from pMF111[16] using *Ssp*I/*Eco*RI into pLMK106 encoding a tTA–AID fusion construct (Karlsson, unpublished). pMK96 (P_{Tet}–avitag–VP16–AID–pA) was constructed by annealing avitag-encoding (underlined) oligos OMK106 (5′-aattcccaccatgggtctgaacgacatcttcgaggctcagaaaatc-gaatggcacgaatccgcgtacagccg-3′) and OMK107 (5′-cgcgcggctgta-cgcggattcgtgccattcgattttctgagcctcgaagatgtcgttcagacccatggt ggg-3′) and directly cloning (*Eco*RI/*Bss*HII) the resulting dsDNA into pMK209. Plasmid pMK82 ($P_{hybrid,TET}$–SEAP–pA) was constructed by transferring SEAP from pMF111 using *Eco*RI/*Not*I into pWW927 (Weber, unpublished) encoding $P_{hybrid,TET}$ originally obtained from ref. 25. Plasmid pMK83 ($P_{EF1\alpha}$–ScbR–VP16–AID–pA) was obtained by amplifying ScbR from pWW122 (oligos OMK101, 5′-gtacggtaccgaattcc-caccatggccaagcaggaccgggcg-3′ and OWW37[18]) and cloning (*Kpn*I/*Bss*HII) into pLMK105 ($P_{EF1\alpha}$–tTA–AID–pA, Karlsson, unpublished). Plasmid pMK86 ($P_{hybrid,ScbR}$–SEAP–pA) was assembled by amplifying $P_{hybrid,ScbR}$ from pWW927 (oligos OMK110, 5′-gatcgtcgactaagatacagactgagcggttttttttcctgcaggtc-gagctcggtacccgggtc-3′ and OWW22[18]) and subsequent cloning (*Sal*I/*Eco*RI) into pWW1088.[34] Plasmid pMK88 ($P_{hybrid,TET}$–Luc–pA) was constructed by transferring Luc from pLMK145 (Karlsson, unpublished) into pMK82 using *Eco*RI/*Not*I. Plasmid pMK127 (P_{PIR8}–Nluc–FRB–pA) was constructed by amplifying Nluc–FRB from pNLuc–FRB[31] (oligos OMK133, 5′-caccgaattccaccatggaagacgccaaaaacataaa-gaaaggc-3′ and OMK134, 5′-ggtggcggccgcttactgctttgagattc-gtcggaacacatg-3′) and subsequent cloning (*Eco*RI/*Not*I) into pBP33.[30] Plasmid pMK130 ($P_{hybrid,TET}$–FKBP12–Cluc–pA) was obtained by amplifying FKBP12–CLuc from pFKBP12–CLuc[31] (oligos OMK135, 5′-caccgaattccaccatgg-gagtgcaggtggaaaccatc-3′ and OMK136, 5′-ggtggcggccgctta-cacggcgatctttccgcccttc-3′) and cloning (*Eco*RI/*Not*I) into pMK82. Plasmids pBP33,[30] pWW804,[35] pWW982 and pWW1023 have been described previously.[29]

Cell culture and transfection

HEK-293T cells were cultivated in DMEM (Invitrogen, Carlsbad, CA, cat. No. P03-0710) supplemented with 10% (vol/vol) FCS (PAN Biotech, Aidenbach, Germany, cat. No. P30-3602, Lot P101003TC) and 1% (vol/vol) penicillin/streptomycin solution (PAN Biotech, Aidenbach, Germany cat. No. P06-07100). For biotin-free conditions FCS was biotin-depleted by incubating with 5 µl streptavidin–agarose suspension

(Novagen, Gibbstown, NJ, cat. No. 69203) per ml FCS at 4 °C overnight. HEK-293T cells were cultivated at 37 °C in a humidified atmosphere containing 5% CO_2 and transfected using an optimized $CaPO_4$-based protocol scaled to one well of a 24-well plate. In brief, 600 ng total DNA (unless stated otherwise, 75 ng of each plasmid were used in the transfection mix for one cell culture well. To complete to 600 ng plasmid DNA per well, a non-coding plasmid (pRSETmod[36]) was added.) in 20 µl 250 mM $CaCl_2$ were dropwise added to 20 µl 2×HBS (50 mM Hepes/NaOH, 280 mM NaCl, 1.5 mM Na_2HPO_4, pH 7.05) under vortexing. After 20 min incubation at room temperature, the DNA precipitate was added to the cells followed by centrifugation at 1200 × *g* for 5 min. After 2 h the medium was exchanged and the appropriate inducer molecules were added. Reporter gene expression was profiled 48 h post-transfection.

Quantification of reporter gene expression

Expression of human placental-secreted alkaline phosphatase (SEAP) was quantified using a *p*-nitrophenylphosphate-based light absorbance kinetic assay as previously described.[24] For quantification of firefly luciferase, cells were lysed by addition of 250 µl (per well of a 24-well plate) luciferase lysis buffer (25 mM Tris/HCl, pH 7.8, 1% Triton X-100, 15 mM $MgSO_4$, 4 mM EGTA, 1 mM DTT). 100 µl of the cell lysate were incubated with a 30 µl firefly luciferase substrate (20 mM Tricine, pH 7–8, 2.67 mM $MgSO_4$, 0.1 mM EDTA, 33.3 mM DTT, 0.52 mM ATP, 0.27 mM Acetyl-CoA, 5 mM NaOH, 50 mM $MgCO_3$, 0.47 mM luciferin). Luciferase activity was monitored with an overall integration time of 10 s using a Synergy™ 4 multi-mode microplate reader (BioTek® Instruments Inc., Winooski, Vermont).

Inducer Molecules

Auxin (indole-3-acetic acid) (Sigma, St. Louis, MO, cat. No. I2886) was dissolved in ethanol as a 1000× stock solution with respect to the final concentration in cell culture medium. Biotin (Acros Organics, Geel, Belgium, cat. No. AC23009) was dissolved in H_2O as a 100× stock dilution. To induce rapamycin-mediated reconstitution of Nluc–FRB with FKBP12–CLuc cells were exposed to 40 nM rapamycin (Calbiochem, Nottingham, UK, cat. No. 553210).

Acknowledgements

We are grateful to Dr Masato Kanemaki (Osaka University) for providing plasmid pNHK60 and Sanjiv Sam Gambhir (Stanford University) for providing plasmids pNLuc-FRB and pFKBP12-CLuc. This work was supported by the Swiss National Science Foundation (Grant No. CR32I3_125426), the European Research Council under the European Community's Seventh Framework Programme (FP7/2007-2013)/ERC Grant agreement no. 259043-CompBioMat and the Excellence Initiative of the German Federal and State Governments (EXC 294 and GSC-4).

References

1 A. Clauset, C. Moore and M. E. J. Newman, *Nature*, 2008, **453**, 98–101.
2 E. H. Davidson, *Nature*, 2010, **468**, 911–920.
3 D. H. Erwin and E. H. Davidson, *Nat. Rev. Genet.*, 2009, **10**, 141–148.
4 E. Ravasz, A. L. Somera, D. A. Mongru, Z. N. Oltvai and A.-L. Barabasi, *Science*, 2002, **297**, 1551–1555.
5 L. N. Booth, B. B. Tuch and A. D. Johnson, *Nature*, 2010, **468**, 959–963.
6 S. B. Carroll, *Cell (Cambridge, Mass.)*, 2008, **134**, 25–36.
7 *Arabidopsis* Interactome Mapping Consortium, *Science*, 2011, **333**, 601–607.
8 A. Herpin, I. Braasch, M. Kraeussling, C. Schmidt, E. C. Thoma, S. Nakamura, M. Tanaka and M. Schartl, *PLoS Genet.*, 2010, **6**, e1000844.
9 V. J. Lynch, R. D. Leclerc, G. May and G. P. Wagner, *Nat. Genet.*, 2011, **43**, 1154–1159.
10 E. H. Davidson and D. H. Erwin, *Science*, 2006, **311**, 796–800.
11 C. Shou, N. Bhardwaj, H. Y. Lam, K. K. Yan, P. M. Kim, M. Snyder and M. B. Gerstein, *PLoS Comput. Biol.*, 2011, **7**, e1001050.
12 N. Dharmasiri, S. Dharmasiri and M. Estelle, *Nature*, 2005, **435**, 441–445.
13 K. Nishimura, T. Fukagawa, H. Takisawa, T. Kakimoto and M. Kanemaki, *Nat. Methods*, 2009, **6**, 917–922.
14 W. Weber, J. Stelling, M. Rimann, B. Keller, M. Daoud-El Baba, C. C. Weber, D. Aubel and M. Fussenegger, *Proc. Natl. Acad. Sci. U. S. A.*, 2007, **104**, 2643–2648.
15 K. Jakobus, S. Wend and W. Weber, *Chem. Soc. Rev.*, 2011, **41**, 1000–1008.
16 M. Fussenegger, R. P. Morris, C. Fux, M. Rimann, B. von Stockar, C. J. Thompson and J. E. Bailey, *Nat. Biotechnol.*, 2000, **18**, 1203–1208.
17 M. Gossen and H. Bujard, *Proc. Natl. Acad. Sci. U. S. A.*, 1992, **89**, 5547–5551.
18 W. Weber, C. Fux, M. Daoud-el Baba, B. Keller, C. C. Weber, B. P. Kramer, C. Heinzen, D. Aubel, J. E. Bailey and M. Fussenegger, *Nat. Biotechnol.*, 2002, **20**, 901–907.
19 W. Weber and M. Fussenegger, *Curr. Opin. Chem. Biol.*, 2011, **15**, 414–420.
20 S. Basu, Y. Gerchman, C. H. Collins, F. H. Arnold and R. Weiss, *Nature*, 2005, **434**, 1130–1134.
21 D. Greber and M. Fussenegger, *Nucleic Acids Res.*, 2010, **38**, e174.
22 T. Sohka, R. A. Heins, R. M. Phelan, J. M. Greisler, C. A. Townsend and M. Ostermeier, *Proc. Natl. Acad. Sci. U. S. A.*, 2009, **106**, 10135–10140.
23 V. Siciliano, F. Menolascina, L. Marucci, C. Fracassi, I. Garzilli, M. N. Moretti and D. di Bernardo, *PLoS Comput. Biol.*, 2011, **7**, e1002074.
24 S. Schlatter, M. Rimann, J. Kelm and M. Fussenegger, *Gene*, 2002, **282**, 19–31.
25 B. P. Kramer and M. Fussenegger, *Proc. Natl. Acad. Sci. U. S. A.*, 2005, **102**, 9517–9522.
26 B. P. Kramer, A. U. Viretta, M. Daoud-El-Baba, D. Aubel, W. Weber and M. Fussenegger, *Nat. Biotechnol.*, 2004, **22**, 867–870.
27 W. Weber, R. Schoenmakers, M. Spielmann, M. D. El-Baba, M. Folcher, B. Keller, C. C. Weber, N. Link, P. van de Wetering, C. Heinzen, B. Jolivet, U. Sequin, D. Aubel, C. J. Thompson and M. Fussenegger, *Nucleic Acids Res.*, 2003, **31**, e71.
28 M. Isalan, C. Lemerle and L. Serrano, *PLoS Biol.*, 2005, **3**, e64.
29 W. Weber, W. Bacchus, F. Gruber, M. Hamberger and M. Fussenegger, *J. Biotechnol.*, 2007, **131**, 150–158.
30 W. Weber, B. P. Kramer, C. Fux, B. Keller and M. Fussenegger, *J. Gene Med.*, 2002, **4**, 676–686.
31 R. Paulmurugan and S. S. Gambhir, *Anal. Chem.*, 2007, **79**, 2346–2353.
32 H. Niwa, J. Miyazaki and A. G. Smith, *Nat. Genet.*, 2000, **24**, 372–376.
33 M. M. Kämpf and W. Weber, *Integr. Biol.*, 2010, **2**, 12–24.
34 W. Weber, C. Lienhart, M. Daoud El-Baba and M. Fussenegger, *Metab. Eng.*, 2009, **11**, 117–124.
35 W. Weber, J. Stelling, M. Rimann, B. Keller, M. Daoud-El Baba, C. C. Weber, D. Aubel and M. Fussenegger, *Proc. Natl. Acad. Sci. U. S. A.*, 2007, **104**, 2643–2648.
36 C. C. Weber, N. Link, C. Fux, A. H. Zisch, W. Weber and M. Fussenegger, *Biotechnol. Bioeng.*, 2005, **89**, 9–17.

